Removal of Cd(II) from Aqueous Solution by Clay-biochar Composite Prepared from *Alternanthera philoxeroides* and Bentonite

Yande Jing,[a,b] Yongqiang Cao,[a,b] Qianqian Yang,[a,b] and Xuan Wang [a,b]

A novel bentonite-biochar (APB) composite was prepared by incorporating bentonite (BE) with *Alternanthera philoxeroides* (AP) biochar for the adsorptive removal of Cd(II) from aqueous media. The APB and the pristine biochar (PB) prepared from the AP were produced at 300 °C under a nitrogen environment. The adsorption capabilities of the BE, PB, and APB were tested for the removal of Cd(II) from aqueous solution. The results showed that the pH substantially affected the adsorption of Cd(II) by the PB and APB. The adsorptive capacity of the Cd(II) onto the PB and APB gradually increased as the pH was increased to 6.0, and there was no significant change in adsorption as the pH was further increased to 8.0. The adsorption kinetic data of the PB and APB were fitted to a pseudo-second-order (PSO) adsorption kinetic model and an intraparticle diffusion (ID) model. The Freundlich model matched the experimental data better than the Langmuir model, indicating that the adsorption was heterogeneous. Thermodynamic study revealed that the adsorption was mainly physisorption, and the adsorption process was endothermic and spontaneous, while the orderliness of all adsorption systems decreased. The results demonstrated that the APB was an effective adsorbent for the removal of Cd(II) from aqueous media.

Keywords: Clay-biochar; Cd(II); Aqueous solution; Removal

*Contact information: a: College of Geography and Tourism, Qufu Normal University, 80 Yantai Road, Rizhao, Shandong, 276826, China; b: Key Laboratory of Nansi Lake Wetland Ecological and Environmental Protection in Universities of Shandong, 57 Jingxuan Road, Jining, Shandong, 273165, China; *Corresponding author: jingyande@163.com*

INTRODUCTION

Cadmium(II) (Cd(II)) pollution has become a severe environmental problem around the world. More than 20,000 tons of Cd(II) enters the environment every year (Hayat *et al*. 2019). The concentration of Cd(II) in heavily polluted waters in China is as great as 4500 µg/L, while the national safety standard for Cd(II) is 0.1 mg/L (GB 8978-1996). Cadmium(II) and its compounds are soluble in water and have high fat solubility, bioaccumulation, and toxicity. They can enter the food chain and ultimately endanger human life and health.

Biochar has a well-developed porous structure. It has good adsorption properties for the removal of heavy metal ions and organic pollutants in water and soil (Ahmad *et al*. 2014; Cao *et al*. 2019). Using biochar to treat heavy-metal-polluted water has attracted wide interest over the past few decades. *Alternanthera philoxeroides* (AP), also known as revolutionary grass, water peanut, or lotus, is an invasive and harmful weed in China's water and terrestrial ecosystem (Holm *et al*. 1977). It has strong resistance, wide adaptability, and rapid reproduction, and its invasion has caused profound harm to the

environment (Li and Liu 2002). Currently, harvested AP is often treated by natural decomposition, which causes secondary environmental problems by releasing pathogens and methane (Xiao *et al*. 2009). However, conversion of the AP into biochar for remediation of heavy-metal-contaminated wastewater can utilize this harmful weed as a resource and avoid secondary pollution, while also expanding the material types of biochar and yielding economic benefits. To the authors' knowledge, little research has been performed on using biochars from AP for the treatment of contaminated media. Only Huang *et al*. (2016) and Yang *et al*. (2014) have made preliminary explorations in this respect. Therefore, it will be of great ecological, environmental, and economic benefit to apply biochar prepared from AP to the remediation of heavy metals in wastewater.

At present, methods of removing Cd(II) from wastewater include extraction, membrane separation, ion exchange, and adsorption, among others (Gupta *et al.* 2009). The central pursuit of the adsorption method is seeking high-performance adsorbents. Recently, porous minerals (including zeolite, bentonite (BE), kaolin, and diatomite) have shown considerable advantages in the preparation of high-performance adsorbents (Wang *et al*. 2015a). Bentonite is a natural, layered, silicate clay mineral with a large specific surface area, excellent adsorption performance, and ion exchange capacity. It can be used for the remediation of heavy metal contamination with good results (Soetaredjo *et al*. 2017). However, BE tends to expand, disperse, and suspend in aqueous solution, and the effect of solid-liquid separation is poor, so it is limited in the treatment of wastewater (Luo *et al*. 2014). To improve the shortcomings of BE, some researchers have prepared a BE-based composite adsorbent and have used it to adsorb heavy metals in water (Fosso-Kankeu *et al*. 2017).

Clay-biochar composite adsorbents have been prepared in previous studies in attempts to increase the amount of pollutants that can be adsorbed compared to the pure adsorbents (Fosso-Kankeu *et al*. 2017). Bentonite-biochar composites have shown reasonably good results in previous studies (Laysandra *et al*. 2018). Previous research (Lee *et al.* 2013; Hao *et al.* 2017) has shown that the nature of the biomass remarkably affects the physicochemical composition of the biochar derived from it. Evidently, a replicate of the above composite with different biomass will exhibit different properties and affinities toward metals. To the authors' knowledge, no studies have examined the application of composite adsorbents from AP and BE for the remediation of Cd(II)-contaminated wastewater. In this study, clay-biochar (APB) composites derived from the AP and BE were prepared at 300 °C, and the obtained composite adsorbents were evaluated for their ability to remove Cd(II) from aqueous solution. Equilibrium and kinetic experiments of Cd(II) adsorption with BE, pristine biochar (PB), and APB were performed. Furthermore, Fourier-transform infrared spectroscopy (FTIR), X-ray diffraction (XRD), and scanning electron microscopy (SEM) were used to characterize the structural differences in the BE, PB, and APB. The effects of pH and temperature were studied. Finally, the mechanisms of Cd(II) removal by the BE, PB, and APB were explored and discussed.

EXPERIMENTAL

Materials

The AP was collected from a pond in Rizhao, Shandong, China (35° 30' N, 119° 16' E). The collected material was cleaned with tap water and then cleaned with deionized water approximately three times. It was placed in a clean and ventilated location for natural

air drying, washed, and oven-dried at 80 °C. Then, it was crushed by a grinder and sieved through a 100-mesh screen for subsequent experiments.

The calcium-based BE was purchased from Henan Yixiang Material Co., Ltd. (Henan, China). After simple physical purification, the calcium-based BE was screened using a 0.15-mm sieve. Reagents were purchased from Tianjin Hengxing Chemical Reagent Co., Ltd. (Tianjin, China). All other chemicals used in these experiments were analytical grade. All solutions were prepared with deionized (DI) water.

Clay-biochar composite preparation

The APB composite was prepared by adapting the procedure used by Yao *et al*. (2014). First, 2 g of the BE powder was dissolved in 500 mL of DI water and treated by sonication (KQ-100V; Kunshan Ultrasonic Instruments Co., Ltd., Kunshan, Jiangsu, China) of the mixture for 30 min to stabilize the BE suspension. Then, 10 g of the AP was weighed, immersed in the BE suspension, and stirred for 2 h. Finally, the feedstocks were separated from the mixture and oven-dried at 80 °C.

The feedstocks were air-dried and ground, packed into a closed ceramic crucibles, and put into a preheated (75 °C) muffle furnace (KSY-12D-16, Longkou City Factory Furnace, Wuhan, China). The feedstocks were decomposed for 2 h at 300 °C in oxygen-limited conditions with the inert atmosphere achieved with an N_2 flow rate of 0.5 L/min. The heating rate was 15 °C/min. After being cooled to room temperature, the solids were cleaned several times with DI water to remove surface impurities and were oven-dried at 80 °C (Wang *et al.* 2015b). The PB, without BE modification, underwent the same pyrolysis process. The obtained adsorbents were ground through a 0.15-mm sieve and stored for later use. The BE-modified biochar and the unmodified biochar were denoted "APB" and "PB," respectively.

Methods

Adsorbent characterization

The surface morphologies and pore structures of the adsorbents were determined using SEM (JSM-5600LV; JEOL Ltd., Tokyo, Japan) at 1000× magnification coupled with an energy dispersive spectroscopy (EDS) instrument (Oxford model 7582, ISIS, USA). Fourier-transform infrared spectroscopy (Tensor 27; Bruker, Karlsruhe, Germany) was used to analyze the surface functional groups of the adsorbents. The adsorbents were ground and mixed with KBr wafers (0.5%). At a 4 cm^{-1} resolution, the spectra were obtained over the range of 500 cm^{-1} to 4000 cm^{-1} with 64 scans. A CHN elemental analyzer (Vario EL Cube; Elementar Analysensysteme GmbH, Langenselbold, Germany) was used to determine the elemental composition (C, H, N, S) of the adsorbents, and the O content was obtained by a mass balance of ash content and elemental contents.

The pH values of the adsorbents were determined as follows: First, 2.5 g of the adsorbent was weighed and added into 50 mL of deionized water. The adsorbent was heated in airtight conditions, boiled for 5 min, and filtered, discarding 5 mL of primary filtrate. The pH of the residual liquid after cooling was measured using a pH meter.

The ash contents of the adsorbents were determined as follows: First, 1.0 g of the adsorbent was weighed and burned in a muffle furnace at 650 °C for 1 hour in aerobic conditions. The ash content was calculated according to the quality of the adsorbents before and after burning.

Adsorption experiments

The adsorption behavior was modeled by three methods: the isotherm model, the kinetic model, and the thermodynamic model. Before applying these models, the adsorption capacity was first determined using Eq. 1,

$$q_t = \frac{(C_0 - C_t)V}{m} \quad (1)$$

where q_t is the amount of Cd(II) adsorbed per unit mass of adsorbent (mg/g), C_0 is the initial concentration of Cd(II) in the solution (mg/L), C_t is the Cd(II) concentration (mg/L) at time t (with the equilibrium concentration also denoted C_e), m is the mass of the adsorbent (g), and V is the solution volume (L).

In the kinetic experiment, the adsorbent dosage was maintained at 0.5 g/L with a Cd(II) concentration of 30 mg/L. The pH of the system was maintained in the range of 7.0 to 8.0. A shaking speed of 200 rpm was maintained during the kinetic experiment. The residence time was varied (5 min, 10 min, 20 min, 30 min, 40 min, 1 h, 1.5 h, 3 h, 6 h, 9 h, 15 h, and 24 h). After each run, the pH values of the suspensions were measured. Then, the concentrations of Cd(II) in the suspensions were determined using an atomic absorption spectrophotometer (GFA-7000A; Shimadzu, Kyoto, Japan) after the suspensions were filtered through a 0.45-μm-filter membrane. Three replications were performed for each contact time. Kinetic modeling was performed using the Origin 9.1 software package (OriginLab, Northampton, MA, USA).

To investigate the adsorption processes of the BE, PB, and APB for Cd(II), different sorption kinetic models were applied to fit the experimental data. These were the pseudo-first-order (PFO) kinetic model (Eq. 2), the pseudo-second-order (PSO) kinetic model (Eq. 3), and the intraparticle diffusion (ID) model (Eq. 4) (Bazrafshan *et al*. 2015),

$$q_t = q_e(1 - e^{-k_1 t}) \quad (2)$$

$$t/q_t = \left(1/k_2 q_e^2\right) + t/q_e \quad (3)$$

$$q_t = k_p\sqrt{t} + c \quad (4)$$

where q_e and q_t are the amounts of Cd(II) adsorbed onto the adsorbent at equilibrium and at time t (mg/g), respectively, k_1 (min^{-1}) and k_2 (g/(mg·min)) are the rate constants of the PFO and PSO adsorption models, respectively, k_p is the ID rate constant (mg/(g·$min^{1/2}$)), and c is the linear intercept.

Adsorption isotherms were determined for different Cd(II) concentrations (20 mg/L, 30 mg/L, 40 mg/L, 50 mg/L, 60 mg/L, 80 mg/L, and 100 mg/L) with a defined pH (pH 7 to 8), adsorbent dosage (0.5 g/L), and residence time (24 h). Other experimental conditions remained similar to the edge and kinetic experiments. The pH values of the suspensions were measured, and the Cd(II) concentrations of the suspensions were analyzed, as described above. Isotherm data for the adsorption of Cd(II) onto the BE, PB, and APB were modeled using the Langmuir (Eq. 5) and Freundlich (Eq. 6) isotherm models,

$$q_e = \frac{q_m K_L C_e}{1 + K_L C_e} \quad (5)$$

$$q_e = K_f C_e^n \quad (6)$$

where K_f (mg/g)·(mg/L)$^{-n}$ and K_L (L/mg) are the Freundlich and Langmuir affinity parameters, respectively, q_e is the equilibrium adsorption capacity (mg/g), C_e is the equilibrium liquid phase concentration (mg/L), q_m is the maximum adsorption capacity in

the Langmuir model (mg/g), and *n* is a Freundlich constant related to adsorption.

To obtain a complete description of the adsorption of Cd(II) onto the BE, PB, and APB, several thermodynamic properties of the adsorption system were assessed. The thermodynamic feasibility of the adsorption of Cd(II) onto the BE, PB, and APB was assessed through the standard Gibbs free energy change ($\Delta G°$, kJ/mol), standard enthalpy change ($\Delta H°$, kJ/mol), and standard entropy change ($\Delta S°$, kJ/(mol·K)). The standard Gibbs free energy change was determined by Eq. 7,

$$\Delta G = -RT \ln K^{o} \quad (7)$$

$$K^{o} = {}^{q_e}/_{C_e} \quad (8)$$

where K^{o} is a thermodynamic distribution coefficient. The value of K^{o} was obtained from Eq. 8 (Khan and Singh 1987), as shown in Eq. 9. The relation between the thermodynamic distribution coefficient and $\Delta H°$ and $\Delta S°$ is given by Eq. 9,

$$\ln K^{o} = -\frac{\Delta G}{RT} = \frac{\Delta S^{o}}{R} - \frac{\Delta H^{o}}{RT} \quad (9)$$

where R is the gas constant (8.314 J/(mol·K)), T is the absolute temperature (K), and K^{o} is the equilibrium constant (m/M). The values of $\Delta H°$ and $\Delta S°$ could be calculated from the slope and intercept of the linear plot of ln K^{o} ($K^{o} = q_e/C_e$) *vs*. $1/T$.

pH-dependent Experiment

The effects of pH changes on Cd(II) adsorption by the BE, PB, and APB were studied by adjusting the pH of 40 mL of Cd(II) solution (30 mg/L) with 0.1 M HNO_3 or NaOH in the pH range of 2.0 to 8.0. Then, 0.02 g of adsorbent was added into a 100-mL centrifugal tube. The concentration of Cd(II) was determined using the atomic absorption spectrophotometer after 24 h by shaking the mixture at 200 rpm at 25 °C. The adsorption capacity of Cd(II) onto the adsorbents at different pH levels was calculated as described above.

RESULTS AND DISCUSSION

Characterization of the Adsorbents

The basic properties of the adsorbents are listed in Table 1. The ash contents of the PB and APB were 14.3% and 19.9%, respectively. The yields of the PB and APB were 50.4% and 56.0%, respectively. The ash content and yield of the APB were greater than those of the PB. This result might have been because the APB had the BE particles attached to the surface of the PB, thus increasing the content of mineral components, such as Si, Mg, and Al in the APB, which increased the content of the APB after pyrolysis (Xu *et al*. 2013). As shown by the elemental compositions of the PB and APB, the most abundant element in the PB and APB was C, followed by O. Such results are consistent with other work (Cao *et al.* 2019). The H/C, O/C, and (O + N) / C ratios are often used to characterize the aromaticity and carbonization degree of adsorbents and the number and polarity of surface oxygen-containing functional groups (Ren *et al*. 2018). As shown in Table 1, the aromaticity of and the number and polarity of oxygen-containing functional groups in the PB were greater than or equal to those of the APB at the same pyrolysis temperature.

The pH values of the PB and APB were all greater than 7, indicating weak alkalinity and mainly being because the PB and APB used AP as a raw material. Organic acids and

phenolic substances were formed due to the decomposition of hemicellulose and cellulose in the AP, which resulted in the pH of adsorbents being near neutrality. Furthermore, the pH of the APB was slightly lower than that of PB. This result was consistent with prior research (Premarathna *et al*. 2019) and was due to the inhibition of the BE adhering to the surface of the AP.

Table 1. Yield, pH, Ash Content, Elemental Composition, and Atomic Ratios

Sample	Yield* (%)	pH	Ash (%)	Elemental Composition (%)					Atomic Ratio		
				N	C	H	S	O	O/C	H/C	(O + N) / C
PB	50.45 ± 0.67	7.35 ± 0.05	14.31 ± 0.43	2.68	47.70	4.19	0.24	30.88	0.65	0.09	0.70
APB	55.97 ± 0.12	7.30 ± 0.15	19.91 ± 0.35	0.77	50.23	4.451	2.73	21.91	0.44	0.09	0.45
BE	—	8.75 ± 0.02	—	—	—	—	—	—	—	—	—
* Data is the mean ± standard deviation based on duplicate measurements											

The SEM images and EDS (energy-dispersive X-ray spectroscopy) analysis of the adsorbents are shown in Fig. 1.

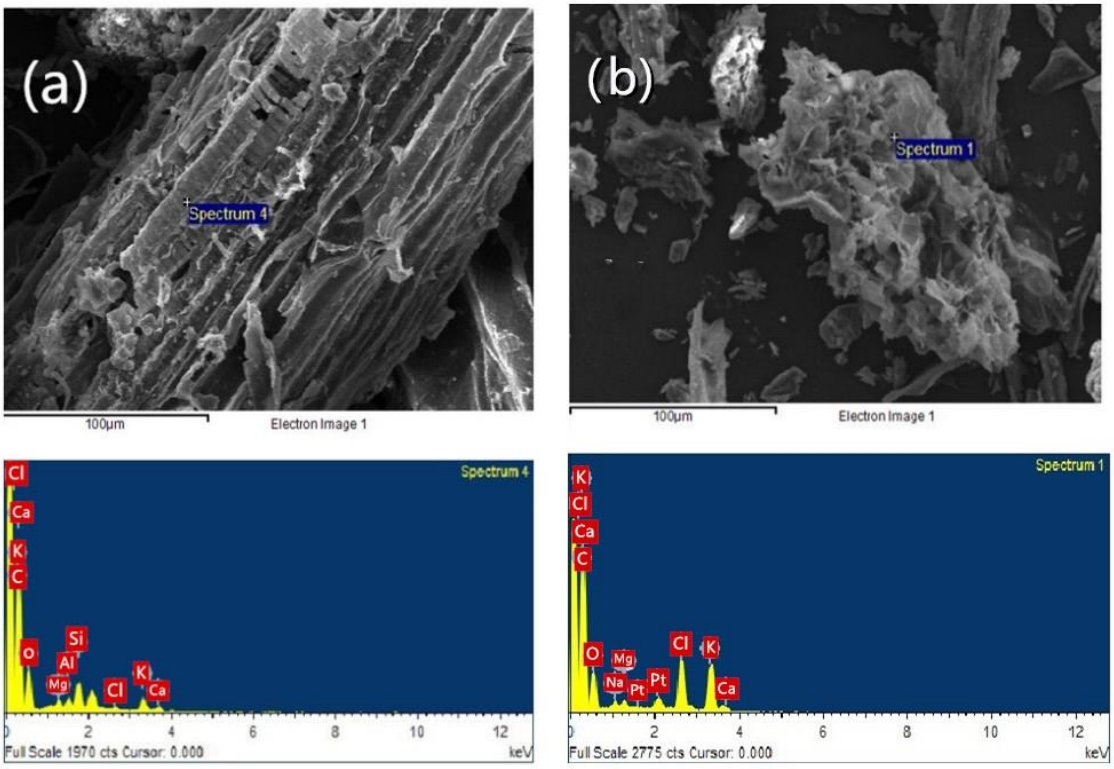

Fig. 1. SEM images and EDS spectra of (a) APB and (b) PB

The SEM results showed that the surface morphologies of the adsorbents varied remarkably between the different types. The PB had a completely tubular or sheet structure with a distinct pore or groove structure on its surface (Wang *et al.* 2019). The surface

morphology of the APB was roughly tubular or of an irregular lamellar structure. The coverage of the BE particles on the surface of the AP biochar was evidenced by the EDS analysis. The BE particles could provide more adsorption sites for the APB. As shown in Fig. 1, compared with the PB, the EDS spectrum of the APB surface showed that the peak values of Si, Ca, Mg, and Al were relatively high, all of which are typical of the elemental composition of montmorillonite, the main component of the BE. This result also shows that the BE was successfully loaded onto the AP biochar.

Fourier-transform infrared spectroscopy was used to qualitatively determinate the functional groups of the BE, PB, and APB. Figure 2 shows the FTIR spectra of the adsorbents. As shown, the types and richness of oxygen-containing functional groups differed greatly among the adsorbents. The stretching vibration absorption peaks of Si-O-Si and Si-O existing in the APB composites were similar to those of the BE, which further indicated that the BE had been loaded onto the surface of the AP biochar.

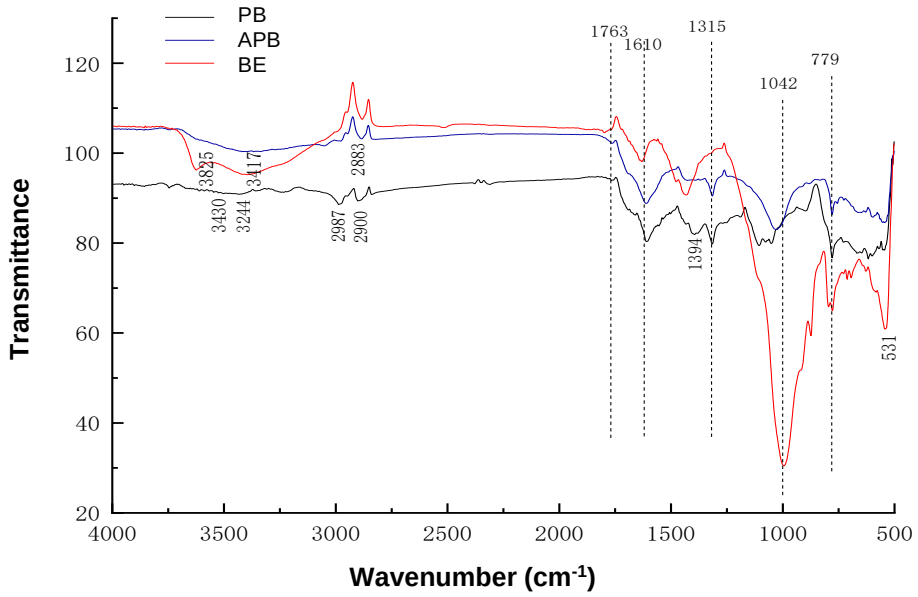

Fig. 2. FTIR spectra of the PB, APB, and BE

The BE exhibited stretching vibration absorption peaks of hydroxyl (-OH) and hydrogen bonds (-OH) at 3625 cm^{-1} and 3417 cm^{-1}, respectively (Paluszkiewicz *et al.* 2008). The absorption peak near 2881 cm^{-1} was caused by the absorption vibration of -CH. The stretching vibration at 1763 cm^{-1} was C=O, and the absorption peaks near 1628 cm^{-1} and 1426 cm^{-1} were -NH bending vibrations. The absorption peaks at 1042 cm^{-1} and 531 cm^{-1} were caused by Si-O stretching vibration and Si-O-Al deformation vibration, respectively, while the absorption peak at 775 cm^{-1} was caused by Si-O-Si stretching vibration (Alabarse *et al.* 2011).

The broad absorption peaks of the PB near 3430 cm^{-1} and 3244 cm^{-1} were caused by the stretching vibrations of phenolic hydroxyls (-OH) (Yu *et al.* 2018; Khan *et al.* 2010). Many absorption peaks near 2839 cm^{-1} to 2987 cm^{-1} were produced by the stretching vibration of aliphatic -CH_2 (Zhang *et al.* 2011). The C-O absorption peak of carboxyl groups was at 1394 cm^{-1}, the C=C stretching vibration peak of aromatic rings was at 1610

cm^{-1} (Zhao *et al.* 2013), and the C-O-C stretching vibration peak of ether in cellulose, hemicellulose, or lignin was at 1047 cm^{-1} (Premarathna *et al*. 2019). The bending vibration absorption peaks of aromatic C-H were mainly located in the wavenumber band from 500 cm^{-1} to 779 cm^{-1}. The absorption peaks near 1610 cm^{-1}, 1394 cm^{-1}, and 1047 cm^{-1} decreased, which indicated that the number of carboxyl, ketone, and ether functional groups was relatively small.

The APB had a stretching vibration absorption peak of -CH near 2883 cm^{-1}, which was similar to that of the PB near this band, indicating that all adsorbents had aliphatic functional groups. The peaks near 1763 cm^{-1} and 1610 cm^{-1} corresponded to the peaks of the PB, which were the stretching vibration of C=O and the stretching vibration of C=C on aromatic rings. Near 1315 cm^{-1} was the stretching vibration peak of C-O, and near 1029 cm^{-1} was the Si-O-Si stretching vibration absorption peak (Ünlü *et al*. 2012). At 780 cm^{-1}, the Si-O-Si stretching vibration absorption peak was similar to that of the BE. These characteristics indicated that the BE had successfully adhered to the surface of the AP biochar.

pH Edge Experiments

The pH of a solution is a major factor that controls adsorption onto adsorbents (Li *et al.* 2017; Premarathna *et al.* 2019). The solution pH affects not only the surface charge of the adsorbents but also the forms and ionization degrees of heavy metals in solution, along with the adsorption rate and degree (Chang *et al.* 2016). When the pH is less than 8.0, Cd(II) mainly exists in the form of free Cd(II) and a small amount of $Cd(OH)^+$ ions in the solution. Greater pH of the solution (pH $\geqslant$ 8) will cause the precipitation of Cd(II) and interfere with the actual adsorption of Cd(II) onto the adsorbents (Chen *et al.* 2011). Therefore, this study examined solution pH in the range of 2 to 8 to test the adsorption of Cd(II) onto the adsorbents. As shown in Fig. 3, the initial pH of the solution had a substantial influence on the adsorption of the Cd(II).

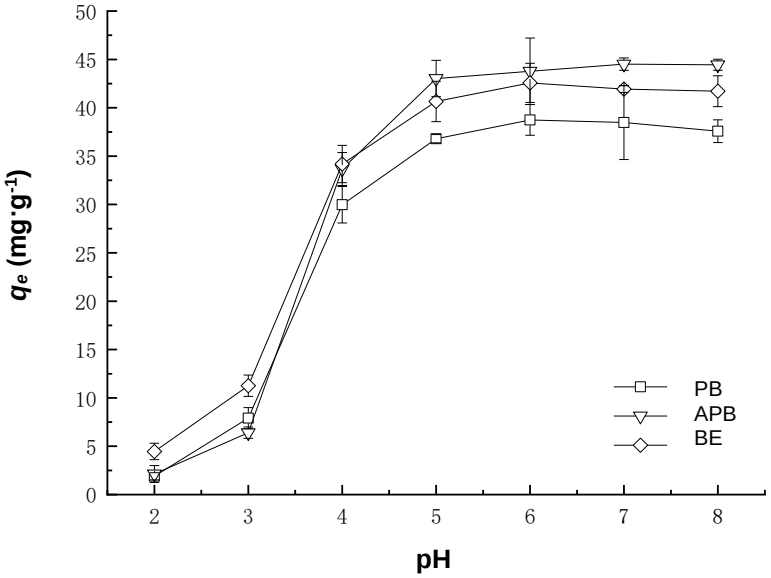

Fig. 3. Effects of initial solution pH on Cd(II) adsorption (Data are the mean ± standard deviation based on duplicate measurements).

Overall, the adsorbed amount of Cd(II) increased rapidly at first and then plateaued with increasing pH. The greatest Cd(II) adsorption by the PB (37.61 mg/g) and APB (44.3 mg/g) was observed at a pH of 6.0. Compared to the PB and APB, the BE showed a similar trend in adsorption capacities in the pH range of 2.0 to 8.0, and the maximum adsorption capacity was similarly obtained at a pH of 6.0. There are three possible reasons for the decreased Cd(II) adsorption capacities at low pH values. First, a large number of H^+ ions and Cd(II) in the solution competed for limited binding sites, which reduced the adsorption of Cd(II). Second, the increased solubility of crystal minerals in the adsorbents resulted in the release of many cations, such as K^+, Ca^{2+}, Mg^{2+}, which competed with Cd(II) in the solution for limited adsorption points. Third, anions, such as CO_3^{2-} and PO_4^{3-}, were difficult to precipitate with Cd(II) in solution. As the solution pH increased, the amount of H^+ in the solution decreased, and the cations (such as K^+, Ca^{2+}, and Mg^{2+}) released by the adsorbent material also decreased, which reduced the competitive adsorption with Cd(II). Moreover, Cd(II) could easily precipitate with anions such as CO_3^{2-} and PO_4^{3-}; thus, the adsorption capacity of Cd(II) onto the adsorbents increased. Moreover, the negative charge density on the surfaces of the adsorbents increased with the increased pH, which was conducive to weakening the electrostatic repulsion of Cd(II) and thus increasing the adsorption capacity (Rivera-Utrilla *et al*. 2013).

Kinetic Experiments

Figure 4 shows the adsorption kinetics curve and models of the Cd(II) adsorption.

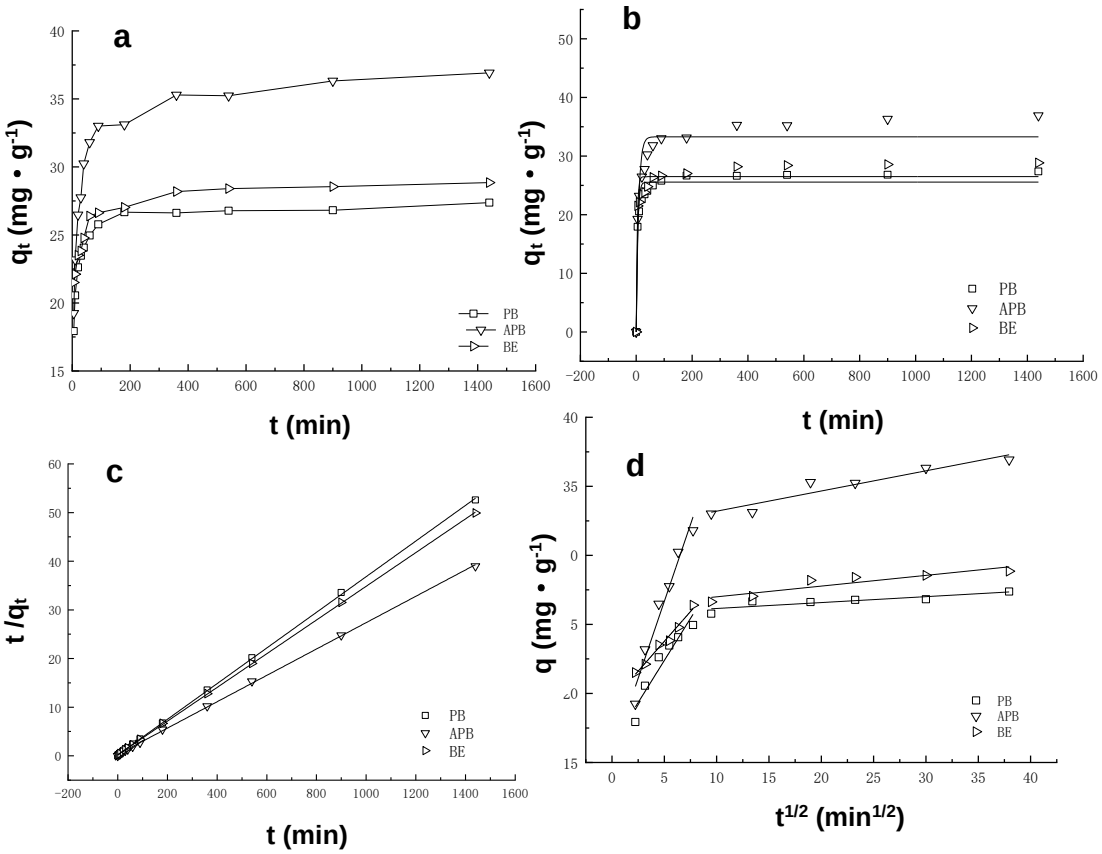

Fig. 4. Kinetic curve and fitted curves of Cd(II) adsorption: (a) kinetics curve, (b) PFO model, (c) PSO model, and (d) ID model

The adsorption process could be divided into two distinct stages. The adsorption capacity of Cd(II) onto the adsorbents increased rapidly with increasing time in the early stage and then plateaued. At 360 min, the adsorption capacities of the BE, PB, and APB to Cd(II) in solution reached 28.2 mg/g, 26.6 mg/g, and 35.3 mg/g, respectively, accounting for more than 95% of the adsorption capacity at 1440 min, basically reaching the equilibrium state of adsorption. The decrease of the active adsorption sites on the adsorbent surfaces caused the decrease of the adsorption rate as time progressed, which caused the adsorption of Cd(II) to diffuse into the adsorbent material.

To better explore the adsorption process and mechanism of Cd(II) and the different adsorbents, based on the analysis of the adsorption kinetics curve, the experimental data were fitted by a PFO kinetic model (Fig. 4b) and a PSO kinetic model (Fig. 4c). The parameters of the PFO and PSO models obtained from the fitting of the experimental data are summarized in Table 2. Both of these models could represent the adsorption kinetic data well, according to the squared correlation coefficients ($R^2 > 0.90$). The R^2 values of the PSO kinetic model were all greater than those of the PFO kinetic model. The theoretical equilibrium adsorption capacities ($q_{e,\,cal}$) of the PSO kinetic model were 27.3 mg/g (PB), 36.9 mg/g (APB), and 28.9 mg/g (BE), which were close to the actual equilibrium adsorption quantities ($q_{e,\,exp}$) of 27.4 mg/g (PB), 36.9 mg/g (APB), and 28.8 mg/g (BE). The PSO model had smaller deviations than the PFO model, which indicated that the PSO kinetic model could better describe the Cd(II) sorption kinetics. It has been shown recently that good fits to the PSO model are generally consistent with diffusion as the rate-limiting process (Hubbe *et al.* 2019).

The parameters k_1 and k_2 reflect the time required for the adsorption process to reach equilibrium in the PFO and PSO kinetic models, respectively (Plazinski *et al*. 2009). These parameters strongly depended on the applied operating conditions, such as temperature, initial concentration, solution pH, and agitation rate. The adsorption rate constant k_2 was greater for PB (0.0072) than for APB (0.0026), and the time required for the PB to reach equilibrium was less than that for the APB. A possible reason was that it took more time and process for Cd(II) to adsorb on the APB due to the BE loading on the surface of the APB.

Table 2. Kinetic Parameters Obtained from PFO and PSO Kinetic Models of Cd(II) Adsorption onto the PB, APB, and BE

Sample	$q_{e,\,exp}$ (mg/g)	PFO Kinetic Model			PSO Kinetic Model		
		$q_{e,\,cal}$ (mg/g)	k_1 (min^{-1})	R^2	$q_{e,\,cal}$ (mg/g)	k_2 (g/(mg·h))	R^2
APB	36.92	33.29 ± 0.99	0.12 ± 0.02	0.9155	36.90 ± 0.71	0.0026 ± 0.0003	0.9997
PB	27.38	25.55 ± 0.50	0.20 ± 0.03	0.9543	27.29 ± 0.81	0.0072 ± 0.0011	0.9999
BE	28.85	26.48 ± 0.64	0.28 ± 0.06	0.9287	28.86 ± 0.11	0.0060 ± 0.0001	0.9999

To determine the actual rate-controlling steps of Cd(II) onto the PB and APB, the ID model was used to fit the experimental data, and the curve in Fig. 4d and the parameters in Table 3 were obtained. The whole adsorption process could be divided into two stages: The first stage (0 min to 60 min) was the process of Cd(II) diffusion onto the surface of the PB and APB, and k_{p1} was greater than k_{p2}, indicating that the boundary diffusion process was fast, and the external surface adsorption was dominant. In the second stage (70 min to

1440 min), the fitting curve plateaued, and k_{p2} was less than k_{p1}, indicating that the adsorption of Cd(II) onto the PB and APB was a rate-controlling step in this stage. As shown in Table 3, the diffusion rate constant k_{p1} was greater than k_{p2}. This result was mainly due to the decrease of Cd(II) concentration in the solution, which led to the decrease of the second stage diffusion rate and the final equilibrium state of Cd(II) adsorption. Meanwhile, the adsorption capacity on the external surface of the adsorbents tended to be saturated in the second stage. With the increase toward the adsorption capacity of the inner surface, the diffusion resistance of Cd(II) increased gradually, which led to a decrease in the diffusion rate. The *C* value in Table 3 indicated the thickness of the adsorbent boundary layer. The *C* value decreased with the increase of heterogeneity and hydrophilic groups on the surfaces of the adsorbents. As shown, C_1 was less than C_2, indicating that the adsorption effect of Cd(II) onto the adsorbents' boundary layers was much greater in the second stage than in the first stage. Figure 4d shows that the adsorption process of the PB and APB for Cd(II) corresponded to multistage linear fitting. None of the straight lines passed through the origin but with positive intercept, indicating that the adsorption process was complicated and had a specific internal diffusion, which might be one of speed-controlling steps. There might be other unknown speed-controlling steps (Ma *et al*. 2011). The actual sorption process included surface adsorption and liquid membrane diffusion, which jointly controlled the adsorption reaction rate (Kara and Tuncel 2011).

Table 3. Parameters of the ID Model for Cd(II) Adsorption

Sample	ID Model					
	k_{p1} (mg/(g·min$^{1/2}$))	C_1	R^2	k_{p2} (mg/(g·min$^{1/2}$))	C_2	R^2
APB	2.23 ± 0.23	15.53 ± 1.19	0.9498	0.19 ± 0.02	30.50 ± 0.55	0.8905
PB	1.22 ± 0.19	16.29 ± 0.99	0.8899	0.04 ± 0.01	25.73 ± 0.28	0.7113
BE	0.86 ± 0.06	19.46 ± 0.29	0.9786	0.08 ± 0.02	26.22 ± 0.41	0.7964

Isotherm Experiments

The isothermal adsorption experiments of Cd(II) onto the adsorbents in solution were performed at 288 K, 298 K, and 308 K. Figure 5 depicts the experimental data fitted by the Freundlich and Langmuir isothermal adsorption models. In Fig. 5, the adsorption experimental data are indicated with symbols, while the solid lines represent the theoretical data from the models. The temperature-dependent parameters obtained from the fitting of the experimental data are summarized in Table 4.

Figure 5 shows that with increasing equilibrium concentration of Cd(II) (C_e), the equilibrium adsorption capacity (q_e) gradually increased, and the growth rate decreased. Furthermore, the actual adsorption capacity of the BE, PB, and APB increased with increasing temperature, which indicated that high temperature was beneficial to the adsorption of Cd(II) onto the BE, PB, and APB, and the adsorption was spontaneous.

Table 4 shows that Freundlich isothermal adsorption model (R^2 = 0.9360 to 0.9932) and the Langmuir isothermal adsorption model (R^2 = 0.8202 to 0.9650) fitted the experimental data of Cd(II) adsorption onto the BE, PB, and APB well. Specifically, the fitting coefficients of the Freundlich model (R^2 = 0.9360 to 0.9932) were greater than those of Langmuir model (R^2 = 0.8202 to 0.9650), which indicated that the Freundlich model could better describe the adsorptive behavior of the Cd(II) onto the adsorbents.

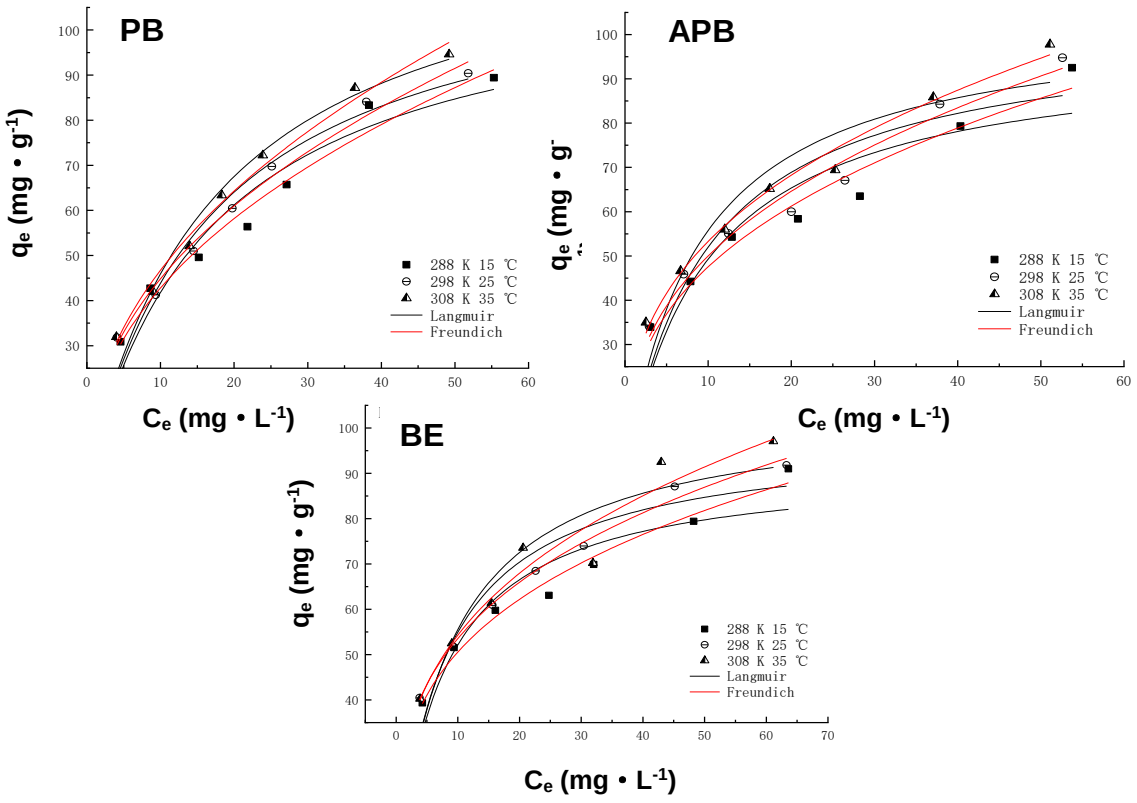

Fig. 5. Adsorption isotherms of Cd(II) at different temperatures

Table 4. Parameters of the Isothermal Sorption Models for Cd(II) Adsorption

Sample	Temperature (K)	Freundlich Model			Langmuir Model		
		K_F (mg/g)·(mg/L)$^{-n}$	n	R^2	q_m (mg/g)	K_L (L/mg)	R^2
PB	288	15.46 ± 1.84	0.4423 ± 0.0346	0.9713	93.89 ± 1.52	0.0581 ± 0.0161	0.9566
	298	16.18 ± 1.32	0.4429 ± 0.0241	0.9861	100.35 ± 0.95	0.0590 ± 0.0122	0.9540
	308	16.22 ± 1.34	0.4598 ± 0.0247	0.9865	103.10 ± 0.94	0.0566 ± 0.0105	0.9650
APB	288	20.49 ± 2.45	0.3655 ± 0.0353	0.9570	97.05 ± 1.32	0.1031 ± 0.0392	0.8202
	298	21.35 ± 2.08	0.3696 ± 0.0291	0.9714	111.94 ± 1.19	0.1042 ± 0.0367	0.8480
	308	23.40 ± 1.58	0.3573 ± 0.0204	0.9848	114.46 ± 1.47	0.1144 ± 0.0376	0.8658
BE	288	20.40 ± 1.73	0.2989 ± 0.0195	0.9789	91.88 ± 0.62	0.1313 ± 0.0369	0.8660
	298	20.57 ± 1.03	0.3011 ± 0.0111	0.9932	107.96 ± 0.21	0.1277 ± 0.0306	0.9056
	308	20.79 ± 3.36	0.3234 ± 0.0377	0.9360	109.42 ± 0.13	0.1137 ± 0.0351	0.8588

The adsorption capacity would continue to increase with the increase of Cd(II) concentration, while there were some inhomogeneities in adsorption. This was consistent with the results of Moyo *et al*. (2016). The non-linear index *n* in the Freundlich model was less than 1, which indicated that the distribution of Cd(II) adsorption sites on the adsorbents were heterogeneous (Fosso-Kankeu *et al*. 2017).

The parameter K_f measures the strength of the attraction and attachment of Cd(II) onto the surface of the adsorbents. The high K_f value indicates that the attraction force was strong. Table 4 shows that K_f increased with increasing temperature, indicating that the adsorptive force of the adsorbents increased with increasing temperature. At 298 K, the adsorption forces of the adsorbents were ordered as follows: APB (21.35) > BE (20.57) > PB (16.18). According to the parameter q_m of the Langmuir model in Table 4, the theoretical maximum adsorption capacities (q_m) for the adsorption of Cd(II) onto the adsorbents were ordered as follows: 111.9 mg/g (APB) > 108.0 mg/g (BE) > 100.4 mg/g (PB), which was the same order as that of the K_f values. The APB had better adsorptive force or capacity for Cd(II) mainly because the surface of the APB contained various functional groups from the bentonite or the AP biochar, and these functional groups enhanced the attraction force of the adsorbents. Furthermore, the loading of the BE onto the APB composite adsorbent increased the adsorptive sites and enhanced ion exchange.

Thermodynamic Experiments

The environmental temperature was one of the main factors affecting adsorption. The experimental data of the Cd(II) adsorption at 288 K, 298 K, and 308 K were analyzed by thermodynamic correlation (Fig. 6). The thermodynamic parameters *KD*, Δ*G*°, Δ*H*°, and ΔS° are summarized in Table 5.

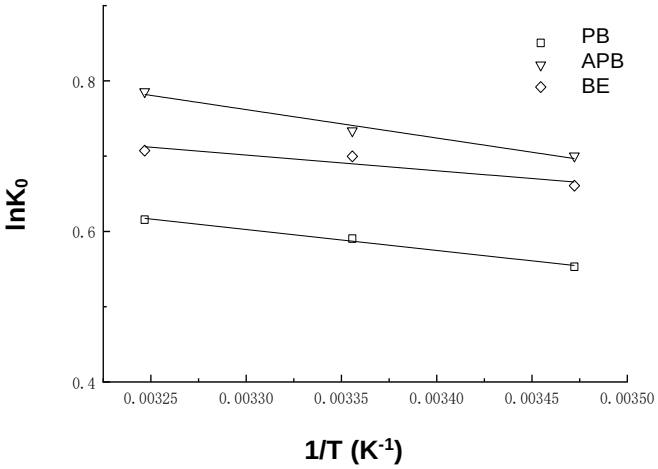

Fig. 6. Effect of temperature on coefficients

The spontaneity of the adsorption process was measured by the standard Gibbs free energy (Δ*G*°). The negative value of Δ*G*° indicates that the adsorption process was spontaneous; the large negative value of Δ*G*° indicates that the system had high adsorption affinity. Table 5 shows that the values of Δ*G*° for the different adsorbents were negative at all three temperatures, which indicated that the adsorbents adsorbed Cd(II) spontaneously.

The values of Δ*G*° decreased with increasing temperature, which indicated that increased temperature was beneficial to the spontaneous adsorption. Generally, values of Δ*G*° in the range of -20 kJ/mol to 0 kJ/mol indicate that physisorption is the primary adsorption process, while chemisorption is the main adsorption process in the range of -400 kJ/mol to -80 kJ/mol (Yu *et al*. 2004). In this study, ΔG° was in the range of -5.50 kJ/mol to -4.07 kJ/mol, indicating that the adsorption process of Cd(II) onto the adsorbents was mainly physisorption.

A positive value of Δ*H*° indicates that an adsorption process is endothermic, and the uptake of adsorbate molecules increases with increasing temperature. A negative value of Δ*H*° indicates that the process is exothermic, and the increased temperature has an adverse effect on the number of adsorbed molecules. The enthalpy change (Δ*H*°) was positive (Table 5), indicating that the adsorption of Cd(II) by the adsorbents at 288 K to 308 K was an endothermic reaction, and the uptake of Cd(II) onto the adsorbents increased with increasing temperature.

The standard entropy change (Δ*S*°) measures the randomness of the adsorption system. A positive value of Δ*S*° shows increased randomness of the interface between adsorbents and adsorbate molecules (Kara and Tuncel 2011; Fil *et al*. 2012), while a negative value of Δ*S*° indicates an increase of orderliness of the adsorption system. With greater order of the system, fewer adsorbate molecules are adsorbed onto the surface of the adsorbents. The values of Δ*S*° were positive for all systems (Table 5), indicating a decrease in the orderliness of all the adsorption systems. The lowest value of Δ*S*° was for BE. This might be because the BE was a clay mineral, which had an ordered crystalline layered structure composed of polymeric sheets of tetrahedral SiO_4 linked into sheets of octahedral $(Al, Mg, Fe)(O, OH)_6$ (Ismadji *et al*. 2015).

Table 5. Thermodynamic Parameters of Cd(II) Sorption

Sample	Δ*G*° (kJ/mol)			Δ*H*° (kJ/mol)	Δ*S*° (kJ/(mol·K))	R^2
	288 K	298 K	308 K			
APB	-4.719	-5.048	-5.496	3.141	16.698	0.9585
PB	-4.073	-4.375	-4.637	2.309	12.629	0.9826
BE	-4.536	-4.880	-5.082	1.729	11.539	0.7628

CONCLUSIONS

1. A novel clay-biochar composite was prepared by thermal treatment of bentonite (BE) and *Alternanthera philoxeroides* (AP) at 300 °C under a nitrogen environment. The SEM and EDS analyses showed that the bentonite-biochar (APB) produced more fragmented substances and had a more developed pore and groove structures than the pristine biochar (PB). The FTIR analysis showed that the stretching vibration absorption peaks of Si-O-Si and Si-O in the APB composites were similar to those in the BE, which indicated that the BE had been loaded onto the surface of the AP biochar.
2. The pH markedly affected the adsorption of the Cd(II) by the PB and APB. The adsorptive capacity of the Cd(II) onto the PB and APB gradually increased with increasing pH in the range of 2.0 to 8.0 and reached equilibrium at a pH of 6.0. The adsorption kinetic data of the PB and APB fitted the PSO adsorption kinetic model and

the ID model, which indicated that the time required for the PB to reach equilibrium was less than that for the APB and the second stage of the adsorption process of Cd(II) onto the PB and APB was the rate-controlling step. The rate of the adsorption reaction might have been controlled by surface adsorption, liquid membrane diffusion, and internal diffusion. The Freundlich model fitted the adsorption isotherm data for all the adsorbents better than the Langmuir model, indicating that the adsorption was a multilayer adsorption process involving, and the distribution of the adsorptive sites of Cd(II) onto the adsorbents was heterogeneous. The thermodynamic study indicated that the adsorption of Cd(II) onto the adsorbents was mainly physisorption, and the adsorption was an endothermic and spontaneous process, while the orderliness of the adsorption system decreased.

3. The APB showed much higher Cd(II) adsorption capacity than the PB and BE. In summary, both waste reuse and Cd(II) removal could been achieved by the APB. The APB could be used as an effective and eco-friendly adsorbent to enhance the removal of Cd(II) from aqueous solution, and it can also provide a theoretical basis for applications in heavy metal pollution remediation from other media.

ACKNOWLEDGMENTS

This research was supported by the Natural Science Foundation of Shandong Province (No. ZR2013DM005) and the Humanities and Social Science General Project of the Ministry of Education (No. 15YJAZH027). The authors extend sincere gratitude to Yongqiang Cao for help in setting up and running the experiments.

REFERENCES CITED

Ahmad, M., Rajapaksha, A. U., Lim, J. E., Zhang, M., Bolan, N., Mohan, D., Vithanage, M., Lee, S. S., and Ok, Y. S. (2014). "Biochar as a sorbent for contaminant management in soil and water: A review," *Chemosphere* 99, 19-33. DOI: 10.1016/j.chemosphere.2013.10.071

Alabarse, F. G., Conceição, R. V., Balzaretti, N. M., Schenato, F., and Xavier, A. M. (2011). "*In-situ* FTIR analyses of bentonite under high-pressure," *Applied Clay Science* 51(1-2), 202-208. DOI: 10.1016/j.clay.2010.11.017

Bazrafshan, A. A., Hajati, S., and Ghaedi, M. (2015). "Synthesis of regenerable $Zn(OH)_2$ nanoparticle-loaded activated carbon for the ultrasound-assisted removal of malachite green: Optimization, isotherm and kinetics," *RSC Adv.* 5(96), 79119-79128. DOI: 1010.1016/j.chemosphere.2013.10.071.1039/C5RA11742A

Cao, Y., Jing, Y., Hao, H., and Wang, X. (2019). "Changes in the physicochemical characteristics of peanut straw biochar after freeze-thaw and dry-wet aging treatments of the biomass," *BioResources* 14(2), 4329-4343. DOI: 10.15376/biores.14.2.4329-4343

Chang, P.-H., Jiang, W.-T., Li, Z., Kuo, C.-Y., Wu, Q., Jean, J.-S., and Lv, G. (2016). "Interaction of ciprofloxacin and probe compounds with palygorskite PFl-1," *J. Hazard. Mater.* 303, 55-63. DOI: 10.1016/j.jhazmat.2015.10.012

Chen, Y. G., Ye, W. M., Yang, X. M., Deng, F. Y., and He, Y. (2011). "Effect of contact time, pH, and ionic strength on Cd (II) adsorption from aqueous solution onto bentonite from Gaomiaozi, China," *Environmental Earth Sciences* 64(2), 329-336. DOI: 10.1007/s12665-010-0850-6

Fil, B. A., Boncukcuoglu, R., Yilmaz, A. E., and Bayar, S. (2012). "Adsorption kinetics and isotherms for the removal of zinc ions from aqueous solutions by an ion-exchange resin," *J. Chem. Soc. Pakistan* 34(4), 841-848.

Fosso-Kankeu, E., Waanders, F. B., and Steyn, F. W. (2017). "Removal of Cr(VI) and Zn (II) from an aqueous solution using an organic-inorganic composite of bentonite-biochar-hematite," *Desalin. Water Treat.* 59, 144-153. DOI: 10.5004/dwt.2016.0059

National information and document Standardization Technical Committee. (1996). "Integrated wastewater discharge standard (GB 8978-1996)," China Standards Press. Beijing.

Gupta, V. K., Carrott, P. J. M., Ribeiro Carrott, M. M. L., and Suhas. (2009). "Low-cost adsorbents: Growing approach to wastewater treatment—A review," *Crit. Rev. Env. Sci. Tech.* 39(10), 783-842. DOI: 10.1080/10643380801977610

Hao, H., Jing, Y.-D., Ju, W.-L., Shen, L., and Cao, Y.-Q. (2017). "Different types of biochar: Effect of aging on the Cu(II) adsorption behavior," *Desalin. Water Treat.* 95, 227-233. DOI: 10.5004/dwt.2017.21524

Hayat, M. T., Nauman, M., Nazir, N., Ali, S., and Bangash, N. (2019). "Environmental hazards of cadmium: Past, present, and future," in: *Cadmium Toxicity and Tolerance in Plants: From Physiology to Remediation*, M. Hasanuzzaman, M. N. V. Prasad, and M. Fujita (eds.), Academic Press, London, UK. DOI: 10.1016/B978-0-12-814864-8.00007-3

Holm, L. G., Plucknett, D. L., Pancho, J. V., and Herberger, J. P. (1977). *The World's Worst Weeds. Distribution and Biology*, University Press of Hawaii, Honolulu, HI, USA.

Huang, X., Liu, Y., Liu, S., Li, Z., Tan, X., Ding, Y., Zeng, G., Xu, Y., Zeng, W., and Zheng, B. (2016). "Removal of metformin hydrochloride by *Alternanthera philoxeroides* biomass derived porous carbon materials treated with hydrogen peroxide," *RSC Adv*. 6(83), 79275-79284. DOI:10.1039/C6RA08365J

Hubbe, M. A., Azizian, S., and Douven, S. (2019). "Implications of apparent pseudo-second-order adsorption kinetics onto cellulosic materials. A review," *BioResources* 14(3), 7582-7626.

Ismadji, S., Soetaredjo, F. E., and Ayucitra, A. (2015). *Clay Materials for Environmental Remediation*, Springer, Cham, Switzerland. DOI: 10.1007/978-3-319-16712-1

Kara, A., and Tuncel, A. (2011). "Kinetics, isotherms and thermodynamics of the adsorption of lead(II) ions onto porous mono-sized microspheres possessing imidazole functional groups," *Adsorpt. Sci. Technol.* 29(3), 259-275. DOI: 10.1260/0263-6174.29.3.259

Khan, A. A., and Singh, R. P. (1987). "Adsorption thermodynamics of carbofuran on Sn (IV) arsenosilicate in H^+, Na^+ and Ca^{2+} forms," *Colloid. Surface.* 24(1), 33-42. DOI: 10.1016/0166-6622(87)80259-7

Khan, S., Rehman, S., Khan, A. Z., Khan, M. A., and Shah, M. T. (2010). "Soil and vegetables enrichment with heavy metals from geological sources in Gilgit, northern Pakistan," *Ecotox. Environ. Safe.* 73(7), 1820-1827. DOI: 10.1016/j.ecoenv.2010.08.016

Laysandra, L., Santosa, F. H., Austen, V., Soetaredjo, F. E., Foe, K., Putro, J. N., Ju, Y.-H., and Ismadji, S. (2018). "Rarasaponin-bentonite-activated biochar from durian shells composite for removal of crystal violet and Cr(VI) from aqueous solution," *Environ. Sci. Pollut. R.* 25(30), 30680-30695. DOI: 10.1007/s11356-018-3104-x

Lee, Y., Park, J., Ryu, C., Gang, K. S., Yang, W., Park, Y.-K., Jung, J., and Hyun, S. (2013). "Comparison of biochar properties from biomass residues produced by slow pyrolysis at 500 °C," *Bioresource Technol.* 148, 196-201. DOI: 10.1016/j.biortech.2013.08.135

Li, X., and Liu, S. (2002). "The harm and prevention and cure of inuasiue of organsiue," *Songliao Journal (Natural Science Edition)* 4, 96-97

Li, Y., Wang, Z., Xie, X., Zhu, J., Li, R., and Qin, T. (2017). "Removal of norfloxacin from aqueous solution by clay-biochar composite prepared from potato stem and natural attapulgite," *Colloid. Surface. A* 514, 126-136. DOI: 10.1016/j.colsurfa.2016.11.064

Luo, P., Zhang, H., Wu, Y., Xu, J., and Tian, Y. (2014). "Preparation of bentonite granule and its adsorption to Cr(VI) in water," *Non-Metallic Mines* 37(2), 72-74, 78.

Ma, Z., Li, Q., Yue, Q., Gao, B., Li, W., Xu, X., and Zhong, Q. (2011). "Adsorption removal of ammonium and phosphate from water by fertilizer controlled release agent prepared from wheat straw," *Chem. Eng. J.* 171(3), 1209-1217. DOI: 10.1016/j.cej.2011.05.027

Moyo, M., Lindiwe, S. T., Sebata, E., Nyamunda, B. C., and Guyo, U. (2016). "Equilibrium, kinetic, and thermodynamic studies on biosorption of Cd(II) from aqueous solution by biochar," *Res. Chem. Intermediat.* 42(2), 1349-1362. DOI: 10.1007/s11164-015-2089-z

Paluszkiewicz, C., Holtzer, M., and Bobrowski, A. (2008). "FTIR analysis of bentonite in moulding sands," *Journal of Molecular Structure* 880(1-3), 109-114. DOI: 10.1016/j.molstruc.2008.01.028

Plazinski, W., Rudzinski, W., and Plazinska, A. (2009). "Theoretical models of sorption kinetics including a surface reaction mechanism: A review," *Adv. Colloid Interfac.* 152(1-2), 2-13. DOI: 10.1016/j.cis.2009.07.009

Premarathna, K. S. D., Rajapaksha, A. U., Adassoriya, N., Sarkar, B., Sirimuthu, N. M. S., Cooray, A., Ok, Y. S., and Vithanage, M. (2019). "Clay-biochar composites for sorptive removal of tetracycline antibiotic in aqueous media," *J. Environ. Manage.* 238, 315-322. DOI: 10.1016/j.jenvman.2019.02.069

Ren, X., Wang, F., Zhang, P., Guo, J., and Sun, H. (2018). "Aging effect of minerals on biochar properties and sorption capacities for atrazine and phenanthrene," *Chemosphere* 206, 51-58. DOI: 10.1016/j.chemosphere.2018.04.125

Rivera-Utrilla, J., Gómez-Pacheco, C. V., Sánchez-Polo, M., López-Peñalver, J. J., and Ocampo-Pérez, R. (2013). "Tetracycline removal from water by adsorption/ bioadsorption on activated carbons and sludge-derived adsorbents," *J. Environ. Manage.* 131, 16-24. DOI: 10.1016/j.jenvman.2013.09.024

Ünlü, C. H., Günister, E., and Atıcı, O. (2012). "Effect of acidity on xylan–montmorillonite bionanocomposites," *Mater. Chem. Phys.* 136(2-3), 653-660. DOI: 10.1016/j.matchemphys.2012.07.038

Wang, X., Jing, Y., Cao, Y., Xu, S., and Chen, L. (2019). Effect of chemical aging of Alternanthera philoxeroides-derived biochar on the adsorption of Pb (II). Water Science and Technology, 80(2), 329-338. DOI: 10.2166/wst.2019.276

Wang, E.-W., Lei, S.-M., Zhang, S.-C., and Huang, T. (2015a). "Purification of the wastewater of quartz processing by mineral-based porous granulation material," *Environm. Sci.* 36(3), 969-979. DOI: 10.13227/j.hjkx.2015.03.028

Wang, R., Zhao, L., Shen, Y., Meng, H., and Yang, H. (2015b). Research progress on preparing biochar and its effect on soil physio-chemical properties. *Journal of Agricultural Science and Technology (Beijing)*, 17(2), 126-133. DOI: 10.13304/j.nykjdb.2014.624

Xiao, L., Yang, L., Zhang, Y., Gu, Y., Jiang, L., and Qin, B. (2009). "Solid state fermentation of aquatic macrophytes for crude protein extraction," *Ecol. Eng.* 35(11), 1668-1676. DOI: 10.1016/j.ecoleng.2008.08.004

Xu, Y.-P., Xie, Z.-B., Zhu, J.-G., Liu, G., and Liu, Q. (2013). "Effects of pyrolysis temperature on physical and chemical properties of corn biochar and wheat biochar," *Soils* 45(1), 73-78.

Yang, Y., Wei, Z., Zhang, X., Chen, X., Yue, D., Yin, Q., Xiao, L., and Yang, L. (2014). "Biochar from *Alternanthera philoxeroides* could remove Pb(II) efficiently," *Bioresource Technol.* 171, 227-232. DOI: 10.1016/j.biortech.2014.08.015

Yao, Y., Gao, B., Fang, J., Zhang, M., Chen, H., Zhou, Y., Creamer, A. E., Sun, Y., and Yang, L. (2014). "Characterization and environmental applications of clay–biochar composites," *Chem. Eng. J.* 242, 136-143. DOI: 10.1016/j.cej.2013.12.062

Yu, Y., Zhuang, Y.-Y., Wang, Z.-H., and Qiu, M.-Q. (2004). "Adsorption of water-soluble dyes onto modified resin," *Chemosphere* 54(3), 425-430. DOI: 10.1016/S0045-6535(03)00654-4

Yu, J., Zhang, X., Wang, D., and Li, P. (2018). "Adsorption of methyl orange dye onto biochar adsorbent prepared from chicken manure," *Water Science and Technology* 77(5), 1303-1312. DOI: 10.2166/wst.2018.003

Zhao, L., Cao, X., Mašek, O., and Zimmerman, A. (2013). "Heterogeneity of biochar properties as a function of feedstock sources and production temperatures," *Journal of Hazardous Materials* 256, 1-9. DOI: 10.1016/j.jhazmat.2013.04.015

Zhang, G., Zhang, Q., Sun, K., Liu, X., Zheng, W., and Zhao, Y. (2011). "Sorption of simazine to corn straw biochars prepared at different pyrolytic temperatures," *Environmental Pollution* 159(10), 2594-2601. DOI: 10.1016/j.envpol.2011.06.012

Article submitted: August 3, 2019; Peer review completed: November 3, 2019; Revised version received: November 30, 2019; Accepted: December 1, 2019; Published: December 4, 2019.
DOI: 10.15376/biores.15.1.598-615